Measurement of acoustic impedance and reflectance in the human ear canal

Susan E. Voss[a] and Jont B. Allen
Acoustics Research Department, AT&T Bell Labs, Murray Hill, New Jersey 07947-2070

(Received 1 January 1993; revised 7 September 1993; accepted 9 September 1993)

The pressure reflectance $R(\omega)$ is the transfer function which may be defined for a linear one-port network by the ratio of the reflected complex pressure divided by the incident complex pressure. The reflectance is a function that is closely related to the impedance of the 1-port. The energy reflectance $\mathscr{R}(\omega)$ is defined as $|R|^2$. It represents the ratio of reflected to incident energy. In the human ear canal the energy reflectance is important because it is a measure of the *in*efficiency of the middle ear and cochlea, and because of the insight provided by its simple frequency domain interpretation. One may characterize the ear canal impedance by use of the pressure reflectance and its magnitude, sidestepping the difficult problems of (a) the unknown canal length from the measurement point to the eardrum, (b) the complicated geometry of the drum, and (c) the cross-sectional area changes in the canal as a function of distance. Reported here are acoustic impedance measurements, looking into the ear canal, measured on ten young adults with normal hearing (ages 18–24). The measurement point in the canal was approximately 0.85 cm from the entrance of the canal. From these measurements, the pressure reflectance in the canal is computed and impedance and reflectance measurements from 0.1 to 15.0 kHz are compared among ears. The average reflectance and the standard deviation of the reflectance for the ten subjects have been determined. The impedance and reflectance of two common ear simulators, the Brüel & Kjaer 4157 and the Industrial Research Products DB–100 (Zwislocki) coupler are also measured and compared to the average human measurements. All measurements are made using controls that assure a uniform accuracy in the acoustic calibration across subjects. This is done by the use of two standard acoustic resistors whose impedances are known. From the experimental results, it is concluded that there is significant subject variability in the magnitude of the reflectance for the ten ear canals. This variability is believed to be due to cochlear and middle ear impedance differences. An attempt was made at modeling the reflectance but, as discussed in the paper, several problems presently stand in the way of these models. Such models would be useful for acoustic virtual-reality systems and for active noise control earphones.

PACS numbers: 43.64.Ha, 43.64.Jb, 43.58.Bh, 43.38.Qf

INTRODUCTION

This paper presents acoustic ear canal impedance and reflectance measurements from 0.1 to 15.0 kHz made on ten subjects, ages 18 to 24, with normal hearing. From our experimental results we conclude that there is significant variability in the magnitude of the impedance and reflectance for the ten ear canals. This conclusion was first reached by Troger (1930). We have attempted to model the reflectance data to explore the nature of the subject variability. For example, one important source of variability in the impedance is due to the variable length of canal between the measurement point and the eardrum.

The ear canal reflectance $R(\omega)$ is defined (Johnson, 1950; Rabbitt, 1990) as the complex ratio of the reflected pressure $P_r(\omega)$ to incident pressure $P_i(\omega)$, and is computed from the normalized ear canal impedance $Z(\omega)=\mathscr{Z}/z_0$ as

$$R(\omega)=\frac{P_r}{P_i} \tag{1}$$

$$=\frac{Z(\omega)-1}{Z(\omega)+1}. \tag{2}$$

In this equation, the ear canal impedance $\mathscr{Z}(\omega)$ has been normalized by the characteristic impedance of the ear canal

$$z_0=\frac{\rho c}{A}, \tag{3}$$

where ρ is the density of air, c is the speed of sound, and A is the (nominal) canal cross-sectional area at the measurement location in the canal. The reflectance R is the transfer function between reflected and incident pressure waves, whereas $Z(\omega)$ is a normalized transfer function between pressure and volume velocity.

The ratio of reflected power $\mathscr{P}_r$ to incident power $\mathscr{P}_i$ is called the *Energy Reflectance* $\mathscr{R}$ (Stinson, 1990); the relation between $\mathscr{R}$ and R is

$$\mathscr{R}=|R|^2. \tag{4}$$

The physical and mathematical properties of $Z(\omega)$ and $R(\omega)$ are quite distinct, and those of R are superior. This is because Z can become singular, whereas R always exists and is always well defined. In a sealed cavity for example, the impedance Z is singular at zero frequency

[a]Present address: Eaton-Peabody Laboratory, Massachusetts Eye and Ear Infirmary, Boston, Massachusetts.

 0001-4966/94/95(1)/372/13/$6.00

($\omega=0$), whereas the reflectance (and the admittance $1/Z$) always exist and are well defined. If one were to excite such a cavity with a pulse of velocity the pressure response approaches 1 as $t\rightarrow\infty$. Such a pressure response has a Laplace transform (for example $1/s$), but it does not have a Fourier transform, and an analysis of such an impedance by numerical Fourier transform methods would be problematic. In the case of an open tube, the reflectance (and in this case the impedance) are well behaved but the admittance has a step response, which again will give trouble at zero frequency. And as a third example, when the real part of a cavity impedance approaches zero, the absorbed energy must approach zero, and neither the impedance or admittance have a Fourier transform because *all* of the poles and zeros of the impedance are on the real frequency axis. In this example, again the reflectance is well behaved. In fact the magnitude of a lossless cavity reflectance approaches one for all frequencies (Johnson, 1950) (i.e., it becomes an all-pass function defined entirely by its phase).

If energy losses due to wave propagation in the ear canal are small, as we believe they are, or when the nonuniformity of the canal is gradual enough so that no significant energy is scattered back, then the energy reflectance at the measurement point and at the eardrum differ only by a phase factor determined by the length of the canal. The magnitude of the impedance, on the other hand, will vary wildly between the same two points, even in a uniform canal.

In a uniform transmission line, the reflectance $R(\omega,x)$ at the termination of the line (the eardrum) at $x=L$ is related to the reflectance at the measurement point (the microphone probe tip) at $x=0$ by the formula

$$R(\omega,L)=R(\omega,0)e^{-2\gamma L}, \tag{5}$$

where γ is the complex wave number for the line (Johnson, 1950), which in general depends on the canal area and frequency. For a lossless uniform line, $\gamma=i\omega/c$, with $i=\sqrt{-1}$. (This formula forms the basis for the well known "Smith chart" used in transmission line theory.)

I. METHODS

Each ear canal impedance measurement consisted of the measurement of seven complex pressure frequency responses, namely of four sealed cavities, two resistor cavities, and the subject's ear. In four subjects repeated measures were made on different days. These collective (seven) measurements took less than 5 min per subject. Each of the individual pressure frequency response measurements took 2.6 s. Four effective (acoustic) lengths L_1 to L_4 for the four cavities were computed from the measured cavity pressures using a least squares gradient procedure (Allen, 1985; Keefe, 1992). Once the acoustic lengths were determined, the cavity impedances were computed using the acoustic lossy-transmission line equations (Keefe, 1984). At each frequency, two earphone Thévenin parameters [the source impedance $Z_s(\omega)$ and the open circuit pressure $P_s(\omega)$, and their Norton equivalents] were found from the four measured cavity pressures and computed cavity load impedances. These Thévenin (Norton) parameters were determined by the least-squares solution of a linear system of over-specified equations (Allen, 1985). This completed the calibration step. To verify the calibration, the impedances of the two resistors were determined from the two resistor pressures and the reflectance was calculated. If the resistor reflectances were within the tolerance range, the subject's canal impedance was computed from the measured canal pressure. If not, the calibration and measurements were repeated.

TABLE I. Table of constants used for calculations.

Name	Constant	Value	Units
Speed of sound	c	33480	cm/s
Density of air	ρ	0.001223	g /cm^3
Canal diameter	d	0.74	cm
Canal area	A	0.43	cm^2
Specific impedance	ρc	40.946	g/s-cm^2
Canal impedance	$z_0=\rho c/A$	95.2	g/s-cm^4

As a second control, repeated measurements were made on four of the subjects. The acoustic impedance of the ear canal depends on the distance between the probe microphone and the eardrum since the ear canal acts as a transmission line. This distance varies from measurement to measurement due to variations of the earplug insertion depth. The magnitude reflectance does not depend on this unknown length or the canal area variation assuming canal losses are small and that area variations are small enough that the reflected energy is negligible. For these reasons the magnitude reflectance should be a more robust measure than the canal impedance for this retest data.

It is theoretically possible to estimate the residual canal length from the slope of the phase of the reflectance at high frequencies. The accuracy of the estimate depends on the range of frequencies over which the reflectance is measured. We will describe this calculation in Sec. II of this paper.

A. Constants

The constants used for all calculations are shown in Table I.

B. Probe insertion depth

To measure the ear canal pressures of the subjects, a foam ear plug (see Fig. 1) containing the two transducer sound tubes was inserted into the subject's ear canal. The aim was to have the entire foam plug fully inserted into the canal so that the rear of the foam plug was flush with the entrance to the canal (flush with the floor of the antitragus). The typical length of a foam plug is 1.2 cm, and the microphone probe tip protruded about 3 mm beyond the lateral edge of the foam plug. This means that the total length of the plug plus the probe is 1.5 cm. *All distances are measured from the microphone probe tip position.* The nominal canal length from the beginning of the canal to the middle of the drum is taken as 2.35 cm (Fletcher, 1925). Due to variations in canal insertion depth, the angle of the

TABLE II. Table of hearing levels (HL) for subjects in dB relative to thresholds for average normals. M=male and F=female indicates the subject's sex. The row labeled AVG HL is the average at each frequency, computed by disregarding the maximum and minimum value at each frequency. It is computed to the nearest 5 dB. The bottom row is the estimated sound pressure level in the ear canal corresponding to the average HL values as determined from the Etymōtic ER-2 data sheet.

		Frequency (kHz)									
Subj	M/F	0.25	0.5	0.75	1.0	1.5	2.0	3.0	4.0	6.0	8.0
1	M	−10	0	5	5	5	0	5	0	0	5
2	M	−10	0	5	5	5	5	−5	0	5	−5
3	F	−10	0	5	5	5	0	0	5	−5	−5
4	M	−5	0	5	5	5	5	0	0	−5	−10
5	F	−10	0	5	5	5	0	10	−5	−10	−10
6	M	5	10	10	10	10	10	0	0	0	10
7	M	−10	0	5	5	5	0	−5	−5	−10	5
8	F	−5	0	5	5	5	0	0	0	−5	−5
9	F	−10	0	0	5	0	0	0	0	−10	5
10	M	5	0	5	5	5	0	0	5	5	10
AVG	HL	−5	0	5	5	5	0	0	0	−5	0
AVG	SPL	14	12	14	14	15	15	15	13	8	14

drum's intersection with the canal, the drum's size, differences in canal length across subjects, and plug length due to compression during the insertion, there will be variation in the distance of the probe from the drum.

High frequency models of the ear canal assume planar wave motions. It is known from theory that nonplanar modes cannot propagate unattenuated for frequencies below the (circular) canal cutoff frequency of 26.5 kHz (Morse and Ingard, 1968, p. 511) because they have a real γ below the cutoff frequency of the canal. If the excitation and measurement points are too close to the drum, nonplanar drum modes can contribute to the pressure. This means that it is important to measure the drum impedance at a canal location far enough from the drum that these nonplanar modes have decayed. Such near-field effects might distort the results. Thus it seems prudent to measure the canal impedance far enough from the drum that these nonplanar modes have been attenuated. The lowest nonplanar mode at 15 kHz is attenuated by $1/e$ within 3.1 mm.

C. Subject threshold measurements

Each subject was tested for hearing thresholds using standard clinical methods (the method of limits), with the same transducer that was used for the impedance measurements. To establish the hearing threshold, the sound level was raised until the subject clearly heard the probe tone. The level was then reduced in 5-dB steps until the subject responded to about 50 percent of the sound presentations. This cycle was repeated several times and the threshold was estimated, within the 5-dB steps. These measurements usually did not take place during the same session as the impedance measurements. The hearing thresholds (in hearing level) are given in Table II.

D. Complex frequency response measurements

The impedance method used here required complex frequency response measurements of the cavities and the ear canal. These measurements were made using SYSid (SYSid is a Trademark of Ariel Corp., Highland Park, NJ), which is a PC software package plus an Ariel DSP–16+ digital signal processing board with 16-bit A/D and D/A analogue IO ports. The software allows for complex frequency response measurements using a chirp signal, with programmable time averaging and FFT lengths. For the measurements made here, the FFT length was 1024 points (12.8 ms), and the signals were averaged 200 times (200×1024 samples, or 2.56 s). The sampling frequency was 40 kHz, giving a sampling period of 25 μs, a maximum frequency of 20 kHz, and a minimum frequency of 39 Hz (40 000/1024). The DC ($\omega=0$) response was not measured. Once the time-averaged response is collected, SYSid Fourier transforms the time response and removes the chirp phase, giving the complex magnitude pressure response of the cavity, resistor, or ear canal.

E. Acoustic calibration

To measure the impedance of the ear canal we determine the Thévenin (Norton) equivalent of the sound delivery system using the four-cavity method. In this method, the complex pressure frequency response of each of the four different cavities is measured, using SYSid. These cavity pressure responses are used to calculate the complex Thévenin (Norton) pressure (velocity) and impedance (admittance) of the sound delivery system. Two additional resistor cavities were used as a control. The cavities and resistors were developed by Mead Killion of Etymōtic Research, and are shown in Figs. 1 and 2. Impedance measurements were made using a sound delivery system which consisted of an Etymōtic ER–2 pressure transducer and an ER–7c probe microphone. Both elements of the sound system are inserted into a foam ear plug which can be inserted into the four cavities or into a human ear canal. Each of the cavities has a diameter of 0.74 cm, which is assumed to be the diameter of the average human ear canal (Shaw, 1978, p. 117). The lengths of cavities C_1, C_2, C_3, and C_4 (see Fig. 1 for the definitions of these lengths) are $L_1=1.13$, $L_2=1.72$, $L_3=2.06$, and $L_4=3.02$ cm, respectively. The physical lengths (and the derived acoustic

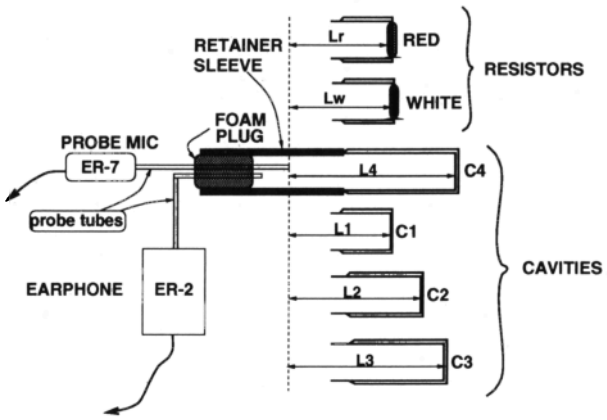

FIG. 1. The calibration system setup. The four cavities are used to calibrate the system, and the two resistor cavities are controls. The foam ear plug containing the sound tubes is calibrated and is then used to measure the human ear canal.

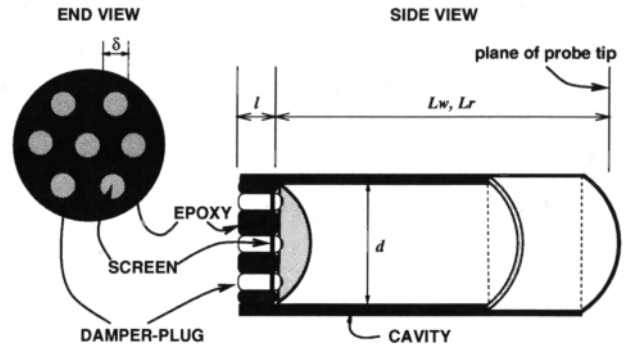

FIG. 2. The red and white resistor cavities each consisted of a main cylindrical cavity terminated with seven acoustical "damper-plugs" mounted into an otherwise closed end. Each damper has a length $l=0.244$ cm and diameter $\delta=0.196$ cm.

lengths) varied slightly, depending on how the foam plug was inserted into the retainer sleeve. For example, for one calibration the derived acoustic lengths are $L_1=1.21$, $L_2=1.78$, $L_3=2.12$, and $L_4=3.07$ cm. Once the Thévenin equivalent parameters P_s and Z_s of the system have been found (as described in the beginning of the Methods section), the unknown ear canal impedance Z_{ec} can be calculated from the pressure P_{ec}, measured with the unknown impedance as the load, using the "pressure divider" equation

$$\frac{P_{ec}}{P_s}=\frac{Z_{ec}}{Z_s+Z_{ec}}. \tag{6}$$

Solving for Z_{ec} this relation is

$$Z_{ec}(\omega)=Z_s(\omega)\frac{P_{ec}(\omega)}{P_s(\omega)-P_{ec}(\omega)}. \tag{7}$$

All impedances displayed in this paper were normalized (divided) by z_0, Eq. (3), rendering them dimensionless.

For sanitary reasons, each subject measurement required a new foam ear plug. Thus it was necessary to recalibrate the system before *each* measurement since the calibration is very sensitive to small changes. For example, one important source of variability was the location of the probe microphone tip, which was approximately 3 mm past the sound delivery tube. Additionally, the foam ear plug was connected to the ER–2 with a short piece of tubing, and the length of this tubing varied slightly with different ear plugs.

F. Impedance calibration controls

In addition to making pressure measurements in the four calibration cavities, control measurements were also made in two resistor cavities, referred to as the red and white resistors. Each resistor cavity is terminated with seven acoustic damper plugs having the configuration shown in Fig. 2. The acoustic dampers are each BF series made by Knowles Electronics, Inc. The red resistor used dampers that have a *red* screen color and are labeled 2200 cgs acoustic ohms. The white resistor used dampers that have a *white* screen color and are labeled 680 cgs acoustic ohms. A mathematical model for each resistor cavity was formulated, and the reflectance for each model was found that matched the reflectance that was experimentally measured using the four-cavity calibration procedure. Since the reflectance of each resistor cavity remained constant over time, this procedure was used as a control on each calibration.

The model is shown in Fig. 3. It consists of a cylindrical piece of tubing with a length and cross-sectional area that is equal to that of the measurement cavity C_1 ($d=0.74$ cm, $L=1.13$ cm). In series with this tube is a representation of the red or white resistor composed of seven acoustic dampers in parallel. Each damper is modeled as a second short piece of transmission line with a resistive screen at one end. The physical diameter of each damper is $\delta=0.196$ cm and the physical length is $l=0.244$ cm. The end correction is not negligible and the acoustic length is the physical length plus the end correction for the side of the plug open to the outside (Beranek, 1954, pp. 132–133). This correction accounts for the radiation impedance. The total acoustic length of a damper used in the model is $l=0.307$ cm. In the model the resistive screen is placed at the entrance to the damper, on the cavity side, to be consistent with the resistor cavity and damper construction. The im-

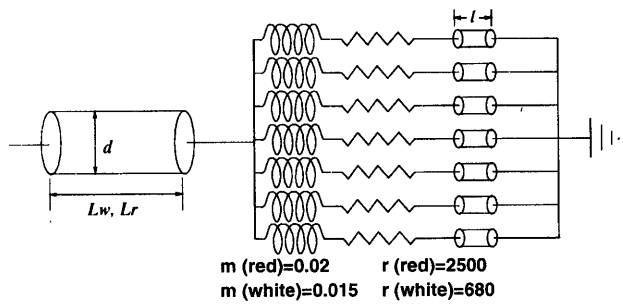

FIG. 3. We show here our equivalent model for the resistors. All units are cgs. The response of this model matches the experimental result of the resistor impedance with an error shown in Fig. 4. Note the difference between the estimated resistance (2500 Ω) and its factory labeled resistance (2200 Ω).

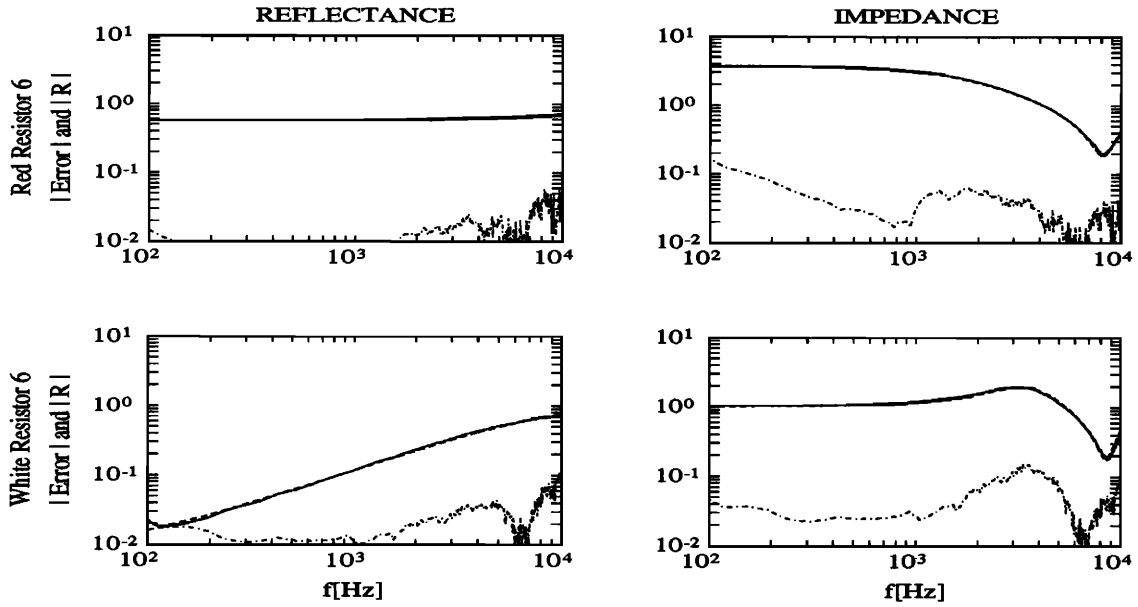

FIG. 4. The solid lines are the model results and the dashed lines (obscured by the solid line) are the experimental results. The lower dash-dot curve in each plot is the absolute error between the experimental result and the model. The impedances have been normalized by z_0.

pedance of each cylindrical tube was modeled by including losses as determined from the approximations given by Keefe (1984). Finally, the model accounts for the change in area between the larger cavity and the seven smaller dampers. This decrease in diameter is represented by a "spreading" inertance (mass) (Karal, 1953; Sondhi, 1983). The original Karal correction series mass (inductance) was not calculated with a boundary condition appropriate for the present situation. However, from the work of Karal, it is clear that there must be some series mass in each of the seven transitions, from a larger to a smaller area, but the value of this mass is not theoretically known. Also any effective mass due to the small holes that make up the resistive screen is not known. Thus in the final empirical model, the parameters for the model of Fig. 3 were adjusted to match the experimental results in both the reflectance and impedance domains. For the red resistor the empirical series mass for each damper was found to be $m=0.02$ H and the resistance was $r=2500\ \Omega$. The white resistor was found to have a series mass of $m=0.015$ H and a resistance of $r=680\ \Omega$ (all units are cgs).

The averaged absolute error of each calibration, from 1000 to 8000 Hz, is defined as

$$E=\frac{1}{U-L+1}\sum_{n=L}^{U}|R(\omega_n)_{\text{measured}}-R(\omega_n)_{\text{model}}| \quad (8)$$

for the reflectance domain and

$$E=\frac{1}{U-L+1}\sum_{n=L}^{U}|Z(\omega_n)_{\text{measured}}-Z(\omega_n)_{\text{model}}| \quad (9)$$

for the impedance domain, where U corresponds to 8000 Hz and L corresponds to 1000 Hz. These limits were used because above 8000 Hz the measured pressure responses of the resistors tended to become noisy. For each calibration the averaged error in the reflectance from Eq. (8) was less than 0.06. The error of the reflectance was used as the standard rather than that of the impedance because the reflectance magnitude is independent of length (ignoring any wall losses). For all the measurements, the largest averaged error across subjects for the red resistor reflectance was 0.033 and the mean averaged error was 0.017. The largest averaged error across subjects for the white resistor reflectance was 0.059 and the mean averaged error of all the experiments was 0.041. A typical comparison of the model reflectance and the resistor reflectance found during the calibration process is shown in Fig. 4. After adjustment of the three parameters of the parametric model, the match to the experimental results is excellent, between 0.1 and 10 kHz. Once the parameters of the model were determined they remained fixed for the duration of the experiment. When the experimental reflectance of the red and white resistors failed to match the model, we assumed there was an error in the calibration process and the calibration was repeated until the match was obtained.

II. RESULTS

The reflectance was computed from the normalized impedance using Eq. (2). This computation indirectly depends on the cross-sectional area of each individual ear canal. Since we did not know the diameter of each ear canal, we used the average diameter of a human ear canal. We checked the reflectance calculation with an area both 20 percent greater and 20 percent less than this average. No Karal correction (spreading inertance) was used for these calculations. Figure 5 shows a comparison of these three reflectance calculations. An error in the assumed canal area affects the magnitude of the reflectance, but the general shape and approximate values of the magnitude of the reflectance remain the same. As a result, it is reason-

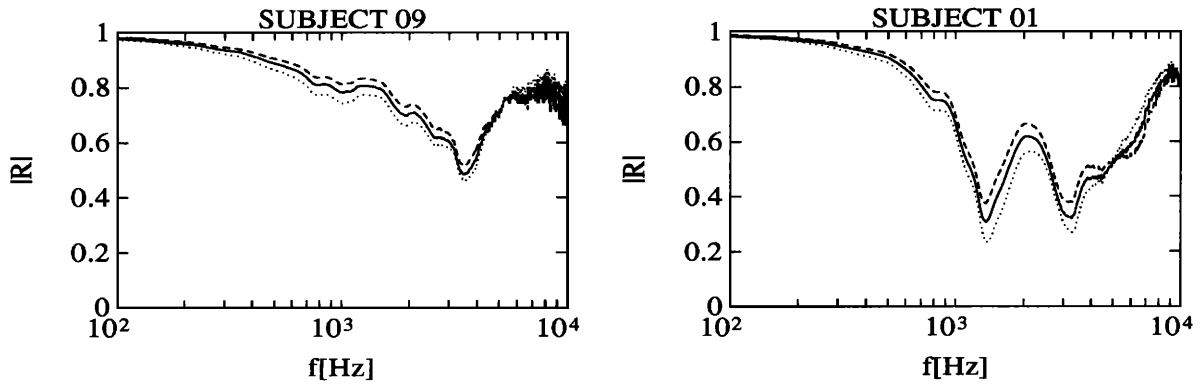

FIG. 5. The solid line shows the reflectance of the two subjects with an average cross-sectional ear canal area. The dotted line is the same reflectance calculated with an area that is twenty percent smaller than average while the dashed line is the reflectance calculated with an area that is twenty percent greater than average.

able to use the average area when one is interested in studying the variability in the reflectance of different human ear canals.

A. Results for the ten subjects

Impedance and reflectance measurements for the ten subjects with normal hearing are shown in Figs. 6–10. In each figure there are two groups of four panels corresponding to a subject. The four panels give the magnitude reflectance (upper left), the reflectance phase and the advanced phase (upper right), the group delay (lower left) and the impedance and advanced impedance (lower right). The graphs with more than one curve (subjects 1, 2, 7, and 9) show test-retest data for that subject. The retest data are shown as a dashed curve in the first panel. Retesting was done on a different day from the original test and with a new foam ear plug and calibration. The remaining three panels refer to the initial measurement (solid curve), not the retest data.

1. Advanced reflectance and impedance

The advanced reflectance phase and the advanced impedance are *advanced* in the sense that they were propagated by a distance L closer to the eardrum, using Eq. (5) with $\gamma = i\omega/c$. This modification had the effect of removing delay from the reflectance, making the advanced phase curve less steep. It was named the *advanced* phase because the corresponding reflectance impulse response has less delay. The advanced impedance was computed using the advanced reflectance and solving for Z in Eq. (2). The advanced impedance is the dashed curve.

The value of L chosen for the figures was somewhat arbitrary (i.e., it is not uniquely determined) but was chosen so that the advanced phase remained between 0 and -2π over the frequency range of the plot. For example, in Fig. 6, $L = 10$ mm for subject 1 and $L = 12$ mm for subject 2, as shown in the title of the phase curve. By plotting the data in this way we hope to extract the most useful information from the curves, yet provide sufficient information to allow one to reconstruct the complex reflectance.

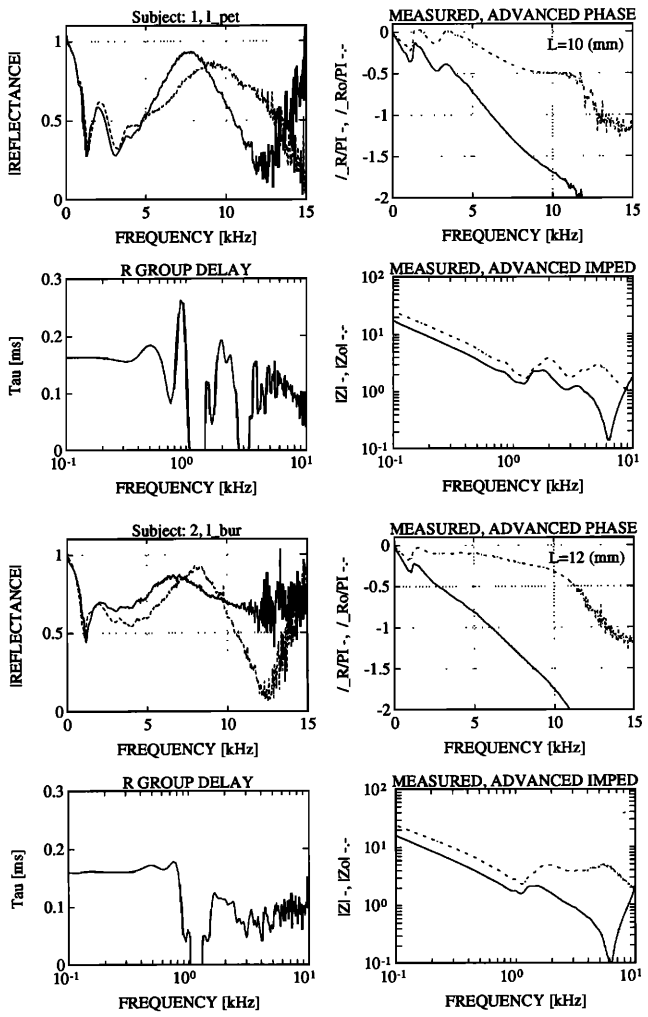

FIG. 6. The upper four panels are the results for subject 1, and the lower four panels correspond to subject 2. Of the four panels, the first one (UPPER LEFT) shows the magnitude pressure reflectance $|R|$. The dashed curve is retest data. The second (UPPER RIGHT) shows two reflectance phase plots, normalized by π radians. The first corresponds to the measured phase data, and the second to the *advanced* phase, derived from Eq. (5) using the L value given at the top of the plot. For subject 1, L was 10 mm. The third curve (LOWER LEFT) is the group delay, which is defined as the negative slope of the measured phase. The fourth curve (LOWER RIGHT) shows the normalized magnitude impedance Z and advanced impedance Z_0 corresponding to the impedance L centimeters closer to the eardrum.

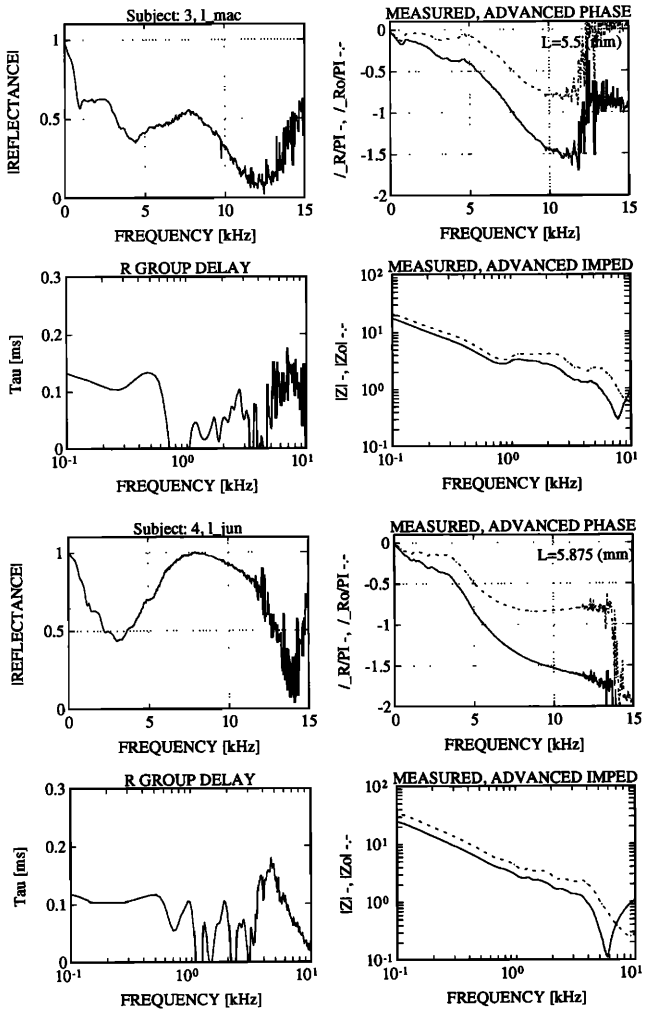

FIG. 7. Same as Fig. 6 for subjects 3 and 4.

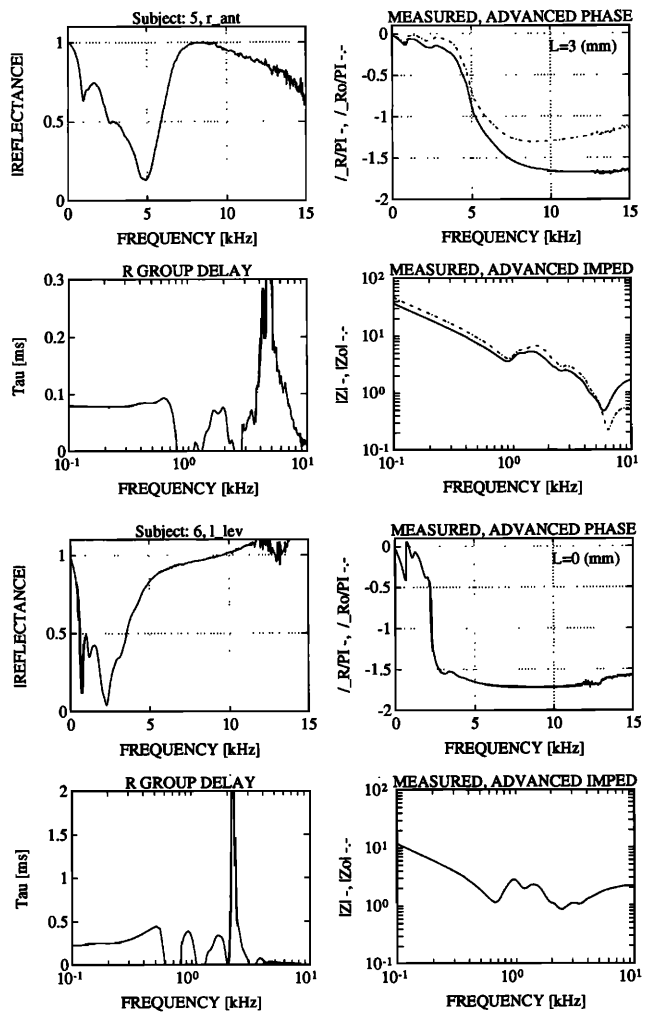

FIG. 8. Same as Fig. 6 for subjects 5 and 6. Note the change in the group delay ordinate for subject 6. Subject 6 is not a typical subject. The reflectance above 10 kHz is greater than 1, indicating experimental calibration or measurement errors for this subject in this frequency range.

There is a great deal of information on these curves and it takes time to become accustomed to reading the plots. In the next sections we describe each panel in greater detail.

2. Magnitude reflectance

The pressure reflectance curves (UPPER LEFT) indicate the inefficiency of the ear, which is given by the square of the values on the curves. Subject 1 for example has $|R|=0.5$ at 5 kHz. This means that 25% of the energy ($100\times0.5^2\%$) is reflected at this frequency. For every subject the reflectance starts at 1 at low frequencies, decreases to a nominal value of 0.6 by about 1 kHz, and then increases to a nominal value of 0.8 by 8 kHz. For all the subjects other than subject 6, it decreases a second time at about 12 kHz. At higher frequencies, where the mass of the middle ear dominates, $|R|$ must approach 1, as is easily seen by substitution of $Z=i\omega m/z_0$ into Eq. (2). Subject 4 shows such a return to 1 for frequencies above 17 kHz. See Sec. III A. for a discussion of this point.

3. Reflectance phase

The curves (UPPER RIGHT) give the phase of the reflectance, in radians, normalized by π (π radians is 180°). These phase plots correspond to the solid curve in the reflectance plot. When retest data are given, the phase for that data is not shown. The two curves shown are related by the relation $\phi_0=\phi+2\omega L/c$, where ϕ is the reflectance phase, and ϕ_o is the propagated (advanced) phase. The value of L is given in the title banner of the phase plot. The advanced reflectance phase always has the lesser slope of the two phase curves, corresponding to a decreased time delay.

4. Reflectance group delay

The group delay shown in this panel is very useful because it has a direct physical interpretation in terms of an effective length, or effective volume. The group delay (LOWER LEFT) is defined as

$$\tau(\omega)=-\frac{\partial\phi}{\partial\omega}, \tag{10}$$

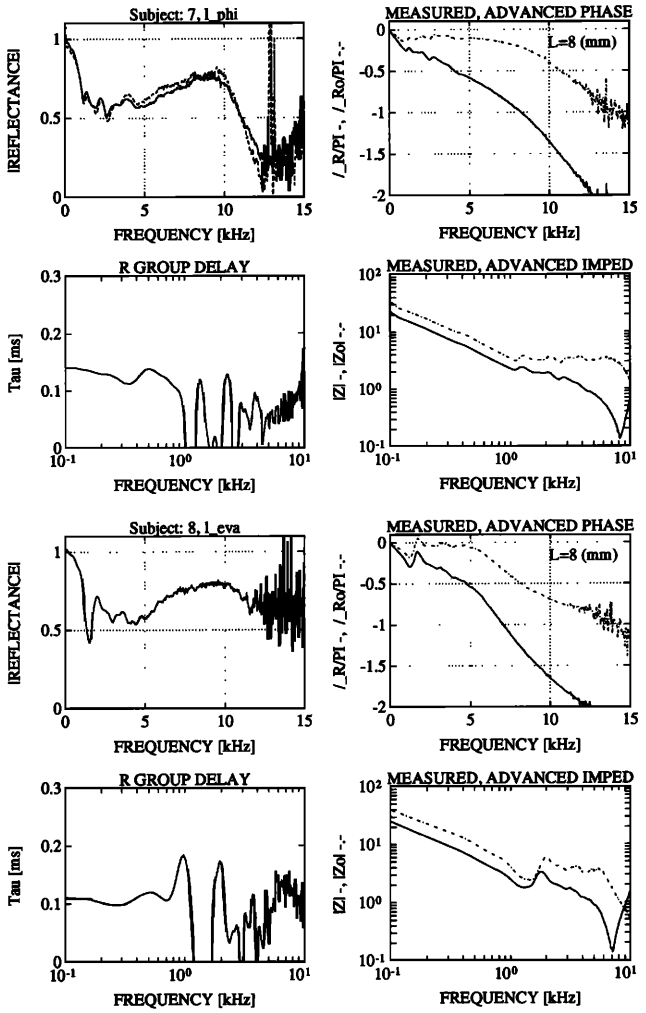

FIG. 9. Same as Fig. 6 for subjects 7 and 8. Subject 7 is a retest subject, so two curves for $|R|$ are shown.

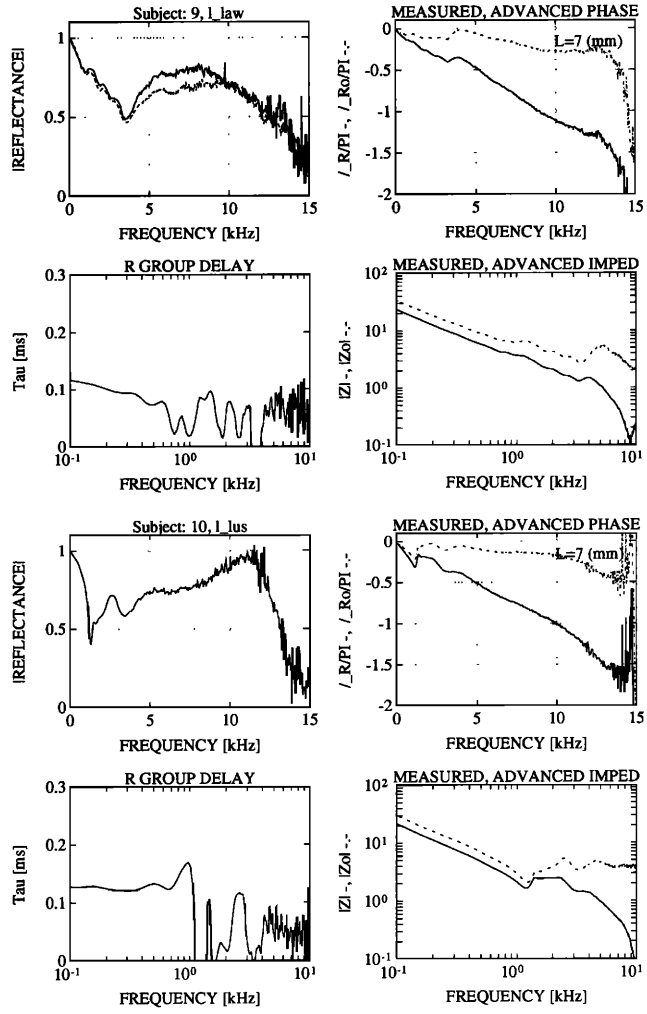

FIG. 10. Same as Fig. 6 for subjects 9 and 10. Subject 9 is a retest subject, so two curves for $|R|$ are shown.

which is the negative of the slope of the phase.

We may obtain important insights about the reflectance group delay at low frequencies ($f<1$ kHz) by modeling the ear canal and drum as an elastic membrane having compliance C_m at the end of a uniform tube with impedance z_0 and length L. From Eq. (2) the reflectance for such a model system is

$$R(\omega,0)=\frac{1-i\omega\tau_m}{1+i\omega\tau_m}e^{-i\omega 2L/c}, \tag{11}$$

where $\tau_m=z_0C_m$. If we compute the group delay τ for this model we find

$$\tau(\omega)=\frac{2L}{c}+\frac{2\tau_m}{1+\omega^2\tau_m^2}. \tag{12}$$

From the group delay shown in the figures for the ten subjects we see a large constant delay at low frequencies, as predicted from Eq. (12). The term $(2L/c)$ of this equation defines a round trip canal delay of 6 μs/mm. This is also the delay seen at the measurement point in the canal at higher frequencies ($f>1/2\pi\tau_m$) when energy is reflected from the eardrum. The second term $(2\tau_m)$ is the group delay due to the eardrum compliance. This term is similar to an electrical "RC" time constant, with the resistance given by $z_0=\rho c/A$ and the compliance of the drum acting as the capacitance. This term shows how the drum compliance makes the canal appear acoustically longer (i.e., larger volume) below a cutoff frequency given by $f_c=1/2\pi\tau_m$. The equivalent canal-drum volume may be computed by multiplication of this effective length by the canal area. *The group delay of the reflectance is therefore an important high frequency generalization of the old idea of an effective canal volume.*

As a consistency check we go through some numbers. Subject 1 Fig. 6 (UPPER LEFT) has a low-frequency group delay of about 175 μs. If the canal is 10 mm long, then the first term of Eq. (12) is 60 μs, and $\tau_m=$ 57.6 μs. This would require an eardrum compliance of $C_m=\tau_m/z_0$, or 0.6×10^{-6}. The impedance for this compliance, at 100 Hz is $1/2\pi fC_m$, which is 2653 Ω. If we divide this impedance by z_0 we find 28, which is the value of the normalized impedance at 0.1 kHz for the advanced impedance (dashed line) for subject 1, Fig. 6 (LOWER RIGHT). Thus in this example, the ratio of the second term to the first term of Eq. (12) was 115/60=1.92, or

almost 2 to 1. When the acoustic length of the canal is less than 10 mm, this ratio will be proportionately larger. The denominator of the second term can be taken as 1 below 1 kHz because $f_c=2.77$ kHz when $2\pi f_c\tau_m=1$.

We would expect the group delay at higher frequencies to be close to the delay corresponding to the acoustic round-trip length $2L/c$, the first term of Eq. (12). For example, subject 2 shows an average delay above 2 kHz of about 90 μs, subject 9 is close to 60, and subject 10, 50 μs. These delays above 2 kHz could well be low level reflections from the drum due to a slight mismatch between the drum impedance and the canal impedance. Other subjects, such as 4 and 5, show resonant like peaks at 5 kHz which are characteristic of resonant structures. We know that a disarticulated stapes can give such effects (Puria, 1991, pp. 98–102) at 8 kHz in the cat.

Subject 6 is clearly different from the other subjects and seems to show resonant effects (i.e., large group delays) across the frequency range from 300 Hz to 3 kHz. While this subject has many uncharacteristic properties in the reflectance phase, the impedance seems near normal, and the hearing thresholds, while within the "normal" range, are the poorest of the group.

5. Impedance and propagated impedance

The two impedance plots are the measured impedance, as measured at the probe microphone tip (solid curve) and the propagated (advanced) impedance (dashed line) estimated at a distance L cm closer to the eardrum, where L is given just below the title banner of the "ADVANCED PHASE" curve (UPPER RIGHT).

At low frequencies (below 1 kHz), the impedance increases after propagation because of the decrease in volume of the canal. At high frequencies the measured impedance is seen to have a null, between 5 and 10 kHz; for example look at subject 1 at 6.1 kHz and subject 7 at 8 kHz. Subject 6 does not show such a dip, perhaps because the probe system was very close to the drum in this subject. The source of this null is commonly attributed to reflections from the eardrum. However it is incorrect to assume that the eardrum is rigid and that the distance to the drum may be estimated from the quarter wavelength formula. This is because the drum reflectance phase at the frequency of the null is not 0 radians, as would be expected from a rigid boundary. In the propagated impedance, the null is effectively removed for many subjects (1, 2, 7, 9, 10), and strongly modified (increased) for many others (3, 4, 8).

B. Coupler reflectance

We measured the impedance and reflectance of both the Brüel & Kjaer 4157 and the Industrial Research Products Inc. DB–100 (Zwislocki) artificial ear couplers. For these measurements, the foam plug was inserted so that the rear of the foam plug was flush with the beginning of the coupler ear canal. Results for both of these ear simulators are shown in Fig. 11.

From the phase and group delay panels of Fig. 11, the canal of the DB–100 seems much shorter than that of the

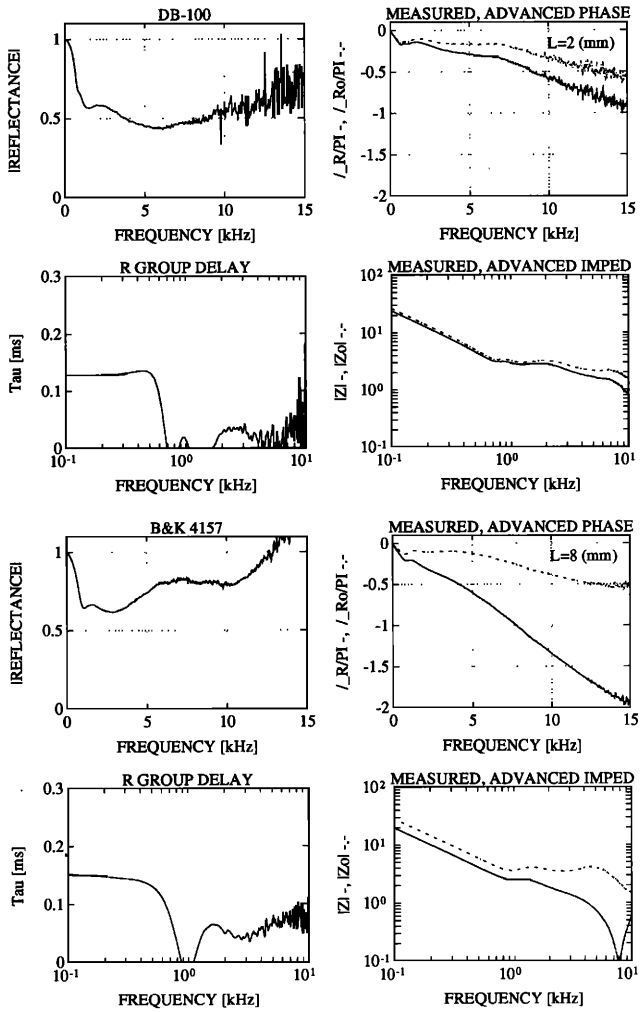

FIG. 11. Same as Fig. 6 for the two ear simulators.

B&K 4157. The magnitude reflectance does not increase at higher frequencies as it does in most human ears and in the 4157. For frequencies above 12 kHz the results for the 4157 are clearly in error because $|R|>1$.

The couplers are compared to the averaged subject data from our ten subjects in Fig. 12 where we see that the DB–100 seems to fit to the average data better below 4 kHz, but the B&K 4157 fits better over the entire 100 Hz to 10 kHz range. The dashed curve in the two panels on the left is the subject reflectance and the dotted curve is the subject standard deviation (s.d.), as a function of frequency. The s.d. may be used to estimate the significance of the differences between the couplers and the averaged reflectance for the ten subjects.

III. DISCUSSION

It is clear from Figs. 6–10 that the reflectance of a human ear canal is quite variable among people with normal hearing. Since there was no tympanometer available when these experiments were performed, the ear canal static air pressure was not known. However, since the between-subject results are repeatable, we feel that this unknown static air pressure is not the only factor in deter-

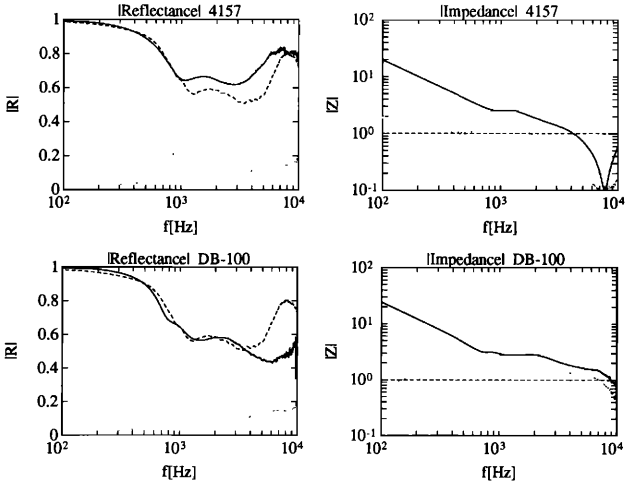

FIG. 12. Magnitude of the impedance and reflectance of the Brüel & Kjaer 4157 and the IRPI DB–100 (Zwislocki) coupler ear simulator (solid curves). The foam ear plug was inserted in each so that it was flush on the outer rim of the ear simulator. In the reflectance plots, the dashed line is the mean reflectance over the ten subjects and the dotted line is the standard deviation. In the impedance plot, the dotted line is the real part of the impedance.

mining the across-subject differences in the reflectance. Since all of the subjects had normal hearing, it is difficult, given the very small threshold variations, to make any conclusions about possible correlations between hearing loss and energy reflectance. The subject with the greatest loss, subject 6, happened to have a phase and group delay that was significantly different from the other subjects, but had the smallest reflectance. This is consistent with resonant structures in the middle ear of this subject which absorb energy at a resonant frequency of 2 kHz. Certainly more data would be required to make further conclusions. Two of the best hearing subjects were 7 and 9 and their reflectances seem typical.

It is interesting to compare our reflectance data to the energy reflectance data of Stinson (1990). Stinson's data were taken by measuring the standing wave pattern in the ear canal for twenty subjects from 3 to 13 kHz. In Fig. 13 we see this comparison. The two results seem similar.

Keefe *et al.* (1993) have studied reflectance in infants and adults. In their results they found the energy reflectance [Eq. (4)] to be 0.95 at 125 Hz, 0.85 at 500 Hz, and dropping to 0.35 from 2 to 4 kHz, and rising to 0.8 at 8 kHz. These results seem similar to those of the present study.

Hudde (1983) measured the impedance and reflectance of six human ears using a two microphone method for frequencies between 1.0 and 20 kHz. He found a reflectance magnitude close to 0.65 for frequencies between 1 and 3 kHz. It then increased to 0.8 at 6 kHz, and was about 0.75 to 0.8 at 10 kHz.

Joswig (1993) has reported canal area function measurements as well as reflectance data. He found $|R|$ to be between 0.5 and 0.6 over the frequency range of 1 to 20 kHz. These results seem inconsistent with ours. It would be interesting to see if the canal area transformation used by Joswig could account for the observed differences.

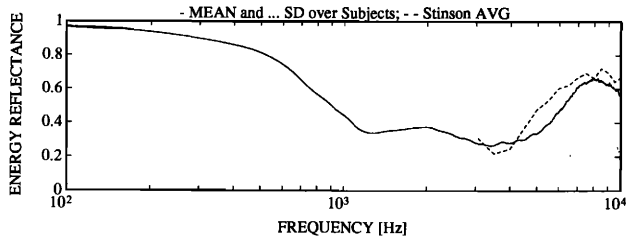

FIG. 13. This figure shows a comparison of the average energy reflectance $\mathscr{R}$ ($N=10$, solid line) and the energy reflectance data of Stinson (1990) ($N=20$, dashed line). The standard deviation of $\mathscr{R}$ is shown as the dotted line.

A. Network properties of an eardrum model

It would be useful to have a model of the human ear canal that would allow one to compute the canal impedance, and its variability, in a systematic and physical manner. Such a model would give us a much needed increased understanding of these data and might be useful in the design of transducers for improved virtual hearing systems and noise cancelling earphones. Readers not interested in such models may wish to skip this section and jump to Sec. III B.

This model might represent an average empirical description of the complex reflectance $R(\omega,L)$ or transmittance $T=1-R$ near the eardrum. The transmittance is the wave transfer function between the transmitted forward wave and the incident forward wave. Given this reflectance or transmittance, one could then compute the impedance for any desired length of canal and canal area, given physical measurements of those quantities. This could be very useful since it would separate the impedance effects due to the cochlea and middle ear from those of the canal. There are some data that indicate that the impedance at the drum may have relatively simple properties [for example, look at the advanced impedance of subject 7, Fig. 9, and the cat data in Allen (1985)].

Such a model is complicated by a particular mathematical property of the reflectance that is somewhat inconvenient, namely its behavior at high frequencies. Because the mass reactance of the drum must dominate the drum impedance at very high frequencies, we know that above about 20 to 30 kHz the drum must scatter almost all of the energy directed at it. This means that at the drum, R must approach 1 above this frequency. To see this use $Z=i\omega m/z_0$ in Eq. (2) and let $\omega\to\infty$. Since $R\to 1$ as $\omega\to\infty$, the inverse Fourier transform of R

$$r(t)=\mathscr{F}^{-1}[R(\omega)] \tag{13}$$

must contain a delta function, corresponding to the high-frequency reflectance from the drum region.

A second problem that we must deal with is the propagation delay in the ear canal. In general this delay can be dispersive (frequency-dependent delay) because of frequency-dependent viscous and thermal losses and gradual changes in area along the length of the canal. As previously described, L must be between 0.5 and 1.0 cm, corresponding to a round-trip delay of 30.0 to 60.0 μs. Since this delay is about one or two sample periods (one time

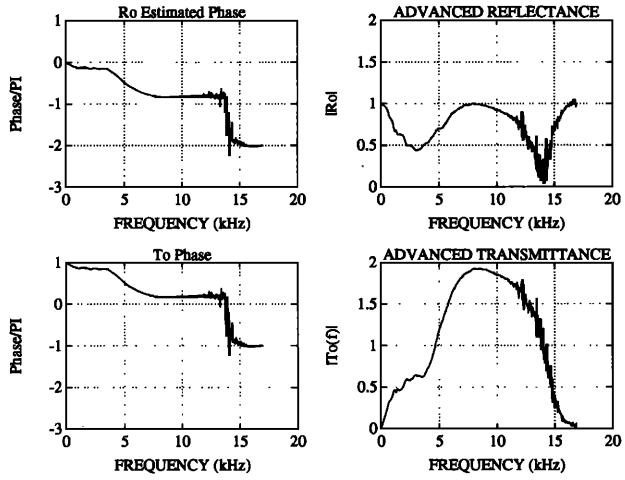

FIG. 14. This figure shows the propagated transmittance $T_0(\omega)$ estimate for subject 4. The reflectance shown in the upper panels was advanced in time by 35.1 μs ($2L=1.175$ *cm*) using Eq. (5). This time shift gave a reflectance phase of 2π radians for frequencies above 15 kHz. Thus for high frequencies above this frequency, $R_0(\omega)=1$. The advanced transmittance $T_0=1-R_0$ phase and magnitude is shown in the lower panels. We will show that the advanced transmittance is a bandpass minimum phase function.

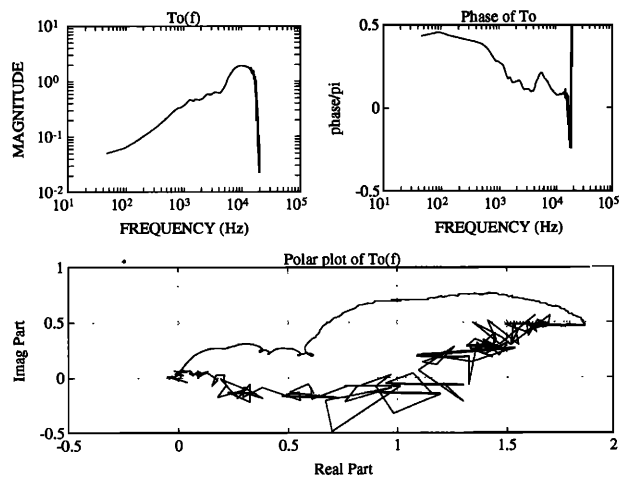

FIG. 15. The advanced transmittance magnitude and phase, and as a polar plot for subject 4. From the polar plot, we see that the transmittance is close to minimum phase, since it does not circle the unit origin, except at high frequencies where its magnitude is very small.

sample corresponds to 25 μs), it follows that any dispersive effects must be small, and hence we ignore them. In the modeling effort presented here we have assumed a uniform canal having no losses ($\gamma=i\omega/c$).

With the problems mentioned above in mind, we propose the following modeling approach. First propagate $R(\omega,0)$ to the eardrum using Eq. (5) with $\gamma=i\omega/c$. We call this reflectance $R_0=R(\omega,L)$ the *propagated* reflectance. To do this requires an estimate of the canal length $\hat{L}$, which is obtained from Eq. (5) by making the phase of R_0 approach a multiple of 2π radians at high frequencies. One may do this only if $|R|$ goes to 1 at high frequencies. Next compute the propagated transmittance $T_0=1-R_0$. Since R_0 approaches 1 both at low frequencies and at high frequencies, T_0 approaches 0, *and is therefore a bandpass function*. The propagated transmittance is a very basic and important function since it is a direct measure of the signal going into the middle ear and cochlea. The propagated impedance Z_0 may also be computed using Eq. (2).

Plots of the estimated R_0 and T_0 for subject 4 are shown in Fig. 14. In this figure R_0 is shown in the upper two panels, and T_0 is shown in the lower two panels. The left panels show the phase after compensating for the estimated length. Note that the phase goes to 2π for frequencies above 15 kHz. The length L in Eq. (5) was varied until the phase at high frequencies was 2π. In this manner, $\hat{L}$ was determined.

1. The transmittance

From a modeling point of view, there is no functional difference between modeling R or T. However from the mathematical point of view, there is a significant difference between these two functions. Every transmittance $T=1-R$ is always minimum phase because

$$T=\frac{2}{Z+1}, \tag{14}$$

which is the ratio of minimum phase functions. Because T is minimum phase, it has different properties than R which is usually not minimum phase.

2. Minimum phase functions

A function $T(\omega)$ is called *minimum phase* if it has no poles or zeros in the right half complex frequency plane, or equivalently, if both T and $1/T$ correspond to causal time responses. For example, every impedance (admittance) is minimum phase. The polar plot of a minimum phase function evulated along ω may never circle the origin, but it may have a real part that is negative.

In Fig. 15 we show the advanced transmittance magnitude and phase for subject 4, along with a polar plot. We see that T_0 is close to minimum phase, except for some high-frequency noise, because it never circles the origin.

a. Problems with the propagated reflectance. There are several problems that are encountered when trying to compute the propagated reflectance. *First*, the method requires high-frequency measurements, which means that the data are noisy because of the small response of the ER–2 above 10 kHz. The source transducer must provide useful output at frequencies where $|R|\to 1$. *Second*, errors in $\hat{L}$ affect the model accuracy. The length estimate follows from the phase of R_0 in a rather straightforward manner. When the wrong value of $\hat{L}$ is used, R_0 will not approach 1 at high frequencies even when $|R|$ does.

b. Noncausal measurements. The *third* problem is the most difficult. When calculating R_0, we discovered to our surprise that for many subjects, $r(t)$ [Eq. (13)], is noncausal. The magnitude of the noncausality is always less than 15 μs, which was less than one sample period. Both the subject measurements, the DB–100, and many of the calibration cavity measurements were so affected. Many calibration cavities and the B&K 4157 coupler had no negative delays.

A simple test to show if a complex frequency response is noncausal is as follows. (a) inverse Fourier transform the frequency response to give the impulse response, $r(t)$; (b) augment the end of the impulse response with zeros; (c) transform back into the frequency domain. If the two magnitude frequency responses are not the same, then the original response was not causal.

After some investigation, we found that R is noncausal because P_{ec}/P_s is noncausal, where P_{ec} is the pressure in a subject's ear and P_s is the Thévenin source pressure found from the calibration.

There are two sources of this problem. The first is when there is significant energy near F_{max}, the maximum frequency, when the phase is not a multiple of π. This condition introduces a fractional sample delay that appears in the time response as samples of the $\sin(t)/t$ function that change sign each sample. This problem may be viewed as aliasing. This type of noncausal effect cannot, in general, be avoided unless the response is "low-pass." The only solution to this problem seems to measure at high enough frequencies so that $T_0 \to 0$.

The second type of possible noncausal response is an "all-pass" factor that is due to a delay of one of the pressures relative to the other. We believe that this second type might appear if there were slight changes in P_s due to the placement of the foam plug in the ear canal. In other words, the calibrations and the resistor controls could be totally free of such error, and yet the Thévenin (Norton) parameters could change slightly as the foam plug is inserted into the canal. If the delay is of the first type it probably should just be ignored since there is nothing that can be done other than increasing the bandwidth of the transducers. If it is of the second type, it could mean there are serious calibration errors. We presently do not know how to distinguish the two types of noncausal delay. The next section is a discussion of this problem in some detail, starting with some definitions from network theory.

3. Positive real functions

A *1-port network* is a "box" with two input wires, such as an inductor or a resistor. A linear time-invariant 1-port network may be characterized by its impedance. For an impedance to be physically realizable, it must be (a) minimum phase and (b) passive. A function $H(\omega)$ is called *minimum phase* if both H and $1/H$ are causal (i.e., the impedance and the admittance must be causal). A 1-port network is *passive* if its real part is non-negative at all frequencies. In network synthesis, a frequency response having these properties is called *positive real* (PR) (Van Valkenburg, 1964, p. 67). Any impedance Z that is PR will have a corresponding R from Eq. (2) that is less than or equal to 1.

If we define H as

$$H=\frac{P_s}{P_{ec}}, \tag{15}$$

then from Eq. (6)

$$H=1+\frac{Z_s}{Z_{ec}}. \tag{16}$$

It follows that H and $H-1$ are minimum phase since they are each equal to the ratio of two impedances, which is always minimum phase but is not, in general, PR. Since this ratio is related to impedances, we may have many of the same singularity problems at $\omega=0$ that impedances and admittances have, meaning we must proceed carefully because we are working with Fourier transforms rather than Laplace transforms. For the case in question H at $\omega=0$ is a positive constant (between 1.0 and 2.5) because both the load and the source are sealed systems which have impedances that approach $K/i\omega$ as $\omega \to 0$. We determined $H(0)$ by the following method. First we inverse transformed $P_s(\omega)$ and $P_{ec}(\omega)$. These time functions were causal and went to 0 as $t \to \infty$. Next we appended zeros to the end of these time functions, and then Fourier transformed back to the frequency domain. In this manner we computed $H(\omega)$ as $\omega \to 0$. Both pressures P_s and P_{ec} will have a large phase shift due to the propagation delay in the source transducer. For H to be minimum phase, the common phase (delay) must exactly cancel. Whenever measurements are made, an antialiasing filter must be used. This filter magnitude and phase will cancel in H.

If H is expanded in a z transform, the leading term $h(0)$ is $1+A_{ec}/A_s$, where A_{ec} is the area of the ear canal and A_s is the area of the calibration cavity. Thus it is very important that H be minimum phase in practice if we hope to compute the area ratio. Since we have observed that H in practice was *not* causal, it follows that either there are fractional sample delays in the response or that P_s has changed slightly due to configuration changes in the foam plug when inserted into the canal. Even if Z_s had changed during insertion, it would still be minimum phase, and the pressure ratio Eq. (6) and Eq. (16) would remain minimum phase. We conclude that testing H and $1/H$ for causality (i.e., testing to see if it is minimum phase) is a strong test for noncausal effects.

4. The magnitude of the noncausal delay

Any transfer function can be factored uniquely into a minimum phase factor M and an all-pass factor A using FFT "cepstral" methods (Oppenheim and Schafer, 1975, p. 504). (This method is called spectral factorization, and is based on a theory mainly developed by Wiener and by Bode in the 1940s.) In other words,

$$H(\omega)=M(\omega)A(\omega). \tag{17}$$

The all-pass factor satisfies the condition $|A|=1$ by definition. This factor is frequently written as $e^{i\phi(\omega)}$, where $i=\sqrt{-1}$ and ϕ is a real function. The all-pass factor uniquely characterizes the nonminimum phase portion of H and may be specified in terms of the group delay of A given by $\tau(\omega)=-\partial\phi/\partial\omega$ if $\phi(0)=0$, as it is here. The group delay of the all-pass portion of Eq. (16) thus gives us frequency specific information about the nonminimum phase behavior of H.

We computed the group delay of the all-pass part of H for the ten subjects and found the following frequency-independent delays: 14, 2, 11, 6, 9.1, 7.5, 6.3, 6.6, 6.7, 2 μs. If the probe tube were to have moved, then to account for these delays it would need to be extended an extra 0.6 to 4.6 mm as it was placed in the canal. Such large distances seem unrealistically large. Thus it seems more likely that the noncausal problem is due to fractional sample delay components in H. Furthermore the close agreement between our average results and those of the DB–100 and the B&K 4157 couplers shown in Fig. 12 suggests that our subject results are correct. However the impedance and reflectance are very sensitive to these delays, we feel that the accuracy of our results could have been affected by any probe movement, which we cannot rule out. Further experimental studies are required to fully understand the significance of this problem.

B. Summary

The ER–2 transducer did not have enough energy at high frequencies to measure the mass dominated region of the drum. Future experiments should try to go to higher frequencies so that the acoustic length of the canal might be estimated from the reflectance. This would also mean that the transmittance would be a low-pass function, which would remove the effect of the fractional sample delay. In general, the reflectance group delay seems like a promising measure of the residual canal length and stiffness. It is a useful high-frequency generalization of the old idea of specifying the equivalent canal volume. Below 1 kHz the delay has two components, one due to the canal length and one due to the drum stiffness. Typically the stiffness gives about twice as much delay as the residual canal length. A simple model of a membrane terminating a tube helped to quantify this effect.

Some subjects showed peaks in the group delay that looked like resonant absorption. In subject 6, who had the poorest hearing thresholds, very large group delays were found. High-frequency dips in the canal impedance were seen, but these dips were not well correlated to the distance from the drum because the phase of the reflectance at the drum is not zero at the dip frequency (it is not rigidly terminated). Thus methods that try to estimate the length of the canal from the frequency of such dips should find poor correlation with the physical length.

We have shown the importance of making high-frequency measurements to allow for the estimate of the canal acoustic length; we have found a powerful test for the validity of the pressure measurements, namely the causality of Eq. (6), and we have outlined a method for modeling the ear canal impedance. This model might be useful in the design of "virtual reality" hearing systems and noise canceling earphones. Because of the frequency response limitations of the ER–2 we have not been successful in modeling these data. An analysis showed that the reflectance measurements of many subjects had a small (e.g., less than 14 μs) noncausal component. The most likely source of this component is fractional sample delay of the energy at high frequencies.

We have explored a method of estimating the eardrum impedance by transforming the impedance into a reflectance, which is then propagated to the eardrum using Eq. (5), with a length determined by the high frequency phase. Estimating the drum impedance in this manner reduces possible interactions of higher drum modes for frequencies below the canal cutoff frequency.

Two ear simulators were measured and compared in Fig. 12 to the average human data. Both simulators were unrealistic at high frequencies (the simulators were not designed to work above 4 kHz, so this is not a negative indication of either simulator). The human reflectance variance was presented on the same graph to help indicate the significance of the differences.

Important properties of the reflectance and transmittance phase were discussed which should be useful in future modeling of the ear canal impedance or reflectance. The propagated transmittance (at the eardrum) is a very basic property since it is a minimum phase measure of the energy transmitted to the middle ear and cochlea.

ACKNOWLEDGMENT

We would like to thank M. M. Sondhi for a great deal of generous help.

Allen, J. B. (1985). "Measurement of eardrum acoustic impedance," in *Peripheral Auditory Mechanisms*, edited by J. B. Allen, J. L. Hall, A. Hubbard, S. T. Neely, and A. Tubis (Springer-Verlag, New York).

Beranek, L. L. (1954). *Acoustics* (McGraw–Hill, New York).

Fletcher, H. (1925). "Useful numerical constants of speech and hearing," Bell Syst. Tech. J. IV(3), 375–386.

Hudde, H. (1983). "Measurement of the eardrum impedance of human ears," J. Acoust. Soc. Am. 73(1), 242–247.

Johnson, W. C. (1950). *Transmission Lines and Networks* (McGraw–Hill, New York).

Joswig, M. (1993). "Impulse response measurement of individual ear canals and impedances at the eardrum in man," Acoustica 77, 270–282.

Karal, F. C. (1953). "The analogous acoustical impedance for discontinuities and constrictions of circular cross section," J. Acoust. Soc. Am. 25, 327–334.

Keefe, D. H. (1984). "Acoustical wave propagation in cylindrical ducts: Transmission line parameter approximations for isothermal and nonisothermal boundary conditions," J. Acoust. Soc. Am. 75, 1386–1391.

Keefe, D. H. (1992). "Method to measure acoustic impedance and reflection coefficient," J. Acoust. Soc. Am. 91, 470–485.

Keefe, D. H., Bulen, J. C., Arehart, K. H., and Burns, E. M. (1993). "Ear-canal impedance and reflection coefficient in human infants and adults," J. Acoust. Soc. Am. 94, 2617–2638.

Morse, P. M., and Ingard, K. U. (1968). *Theoretical Acoustics* (McGraw–Hill, New York).

Oppenheim, A. V., and Schafer, R. W. (1975). *Digital Signal Processing* (Prentice-Hall, Engelwood Cliffs, NJ).

Puria, S. (1991). "A theory of cochlear input impedance and middle ear parameter estimation," Ph.D. thesis, City University of New York.

Rabbitt, R. D. (1990). "A hierarchy of examples illustrating the acoustic coupling of the eardrum," J. Acoust. Soc. Am. 87, 2566–2582.

Shaw, E. A. G. (1978). "The acoustics of the external ear," in *Acoustical Factors Affecting Hearing Aid Performance*, edited by G. A. Studebaker and I. Hochberg (University Park, Baltimore, MD), pp. 109–125.

Sondhi, M. M. (1983). "An improved vocal tract model," Proc. Int. Conf. Acoust., Paris 4, 167–170.

Stinson, M. (1990). "Revision of estimates of acoustic energy reflectance at the human eardrum," J. Acoust. Soc. Am. 88(4), 1773–1778.

Tröger, J. (1930). "Die schallaufnahme durch das äussere ohr.," Physik Z. 31, 26–47.

Van Valkenburg, M. E. (1964). *Modern Network Synthesis* (Wiley, New York).